AD

AD-E401 102

TECHNICAL REPORT ARLCD-TR-83047

CARS SPECTROSCOPY OF PROPELLANT FLAMES

L. E. HARRIS

DTIC
ELECTE
S
NOV 1 7 1983
D
A

NOVEMBER 1983

U.S. ARMY ARMAMENT RESEARCH AND DEVELOPMENT CENTER

LARGE CALIBER WEAPON SYSTEMS LABORATORY

DOVER, NEW JERSEY

APPROVED FOR PUBLIC RELEASE; DISTRIBUTION UNLIMITED.

83   004

REPORT DOCUMENTATION PAGE		READ INSTRUCTIONS BEFORE COMPLETING FORM
1. REPORT NUMBER Technical Report ARLCD-TR-83047	2. GOVT ACCESSION NO. AD-A134990	3. RECIPIENT'S CATALOG NUMBER
4. TITLE *(and Subtitle)* CARS SPECTROSCOPY OF PROPELLANT FLAMES		5. TYPE OF REPORT & PERIOD COVERED Final
		6. PERFORMING ORG. REPORT NUMBER
7. AUTHOR(s) L. E. Harris		8. CONTRACT OR GRANT NUMBER(s)
9. PERFORMING ORGANIZATION NAME AND ADDRESS ARDC, LCWSL Applied Science Div [DRSMC-LCA-G(D)] Dover, NJ 07801		10. PROGRAM ELEMENT, PROJECT, TASK AREA & WORK UNIT NUMBERS 1L161122AH60
11. CONTROLLING OFFICE NAME AND ADDRESS ARDC, TSD STINFO Div [DRSMC-TSS(D)] Dover, NJ 07801		12. REPORT DATE November 1983
		13. NUMBER OF PAGES 36
14. MONITORING AGENCY NAME & ADDRESS*(If different from Controlling Office)*		15. SECURITY CLASS. *(of this report)* Unclassified
		15a. DECLASSIFICATION/DOWNGRADING SCHEDULE

16. DISTRIBUTION STATEMENT *(of this Report)*

Approved for public release; distribution unlimited.

17. DISTRIBUTION STATEMENT *(of the abstract entered in Block 20, if different from Report)*

18. SUPPLEMENTARY NOTES

Presented at the Ninth International Colloquium on Dynamics of Explosives and Reactive Systems, Poitiers, France, July 1983.

19. KEY WORDS *(Continue on reverse side if necessary and identify by block number)*
Broadband CARS
CARS spectra
Spectroscopy
Propellant

20. ABSTRACT *(Continue on reverse side if necessary and identify by block number)*

Obtaining useful experimental information on the dynamics of the deflagration and detonation of energetic materials has been difficult with conventional techniques. The advent of nonlinear techniques such as coherent anti-stokes Raman scattering (CARS) provides an opportunity to extend the information obtainable on these energetic systems. Propellant flames are often transient, particle-laden, and turbulent. Single-shot nitrogen CARS spectra from propellant flames demonstrated the direct applicability of CARS in obtaining

(cont)

DD, FORM 1473 EDITION OF 1 NOV 65 IS OBSOLETE

20. ABSTRACT: (cont)

temperature and concentration in propellant flames. Further investigations were also made of model propellant flames such as CH_4/N_2O to assess the range of applicability of CARS in studies of the combustion of propellants and other reactive systems.

Broadband CARS spectra were obtained from both the reaction zone and post-flame region of CH_4/N_2O flames. The temperature and concentration profiles obtained from both N_2 and N_2O CARS spectra were used to understand the elementary processes occurring in CH_4/N_2O flames. In addition, N_2 and CO vibrational CARS spectra obtained from the post-flame region of CH_4/N_2O flames were used to obtain concentration and temperature profiles by a least-square fit to model calculations. The results obtained were in accord with thermochemical calculations. In rich CH_4/N_2O flame previously unobserved, CARS spectra were obtained from several pure rotational H_2 transitions. These H_2 spectra offer further opportunities for studying propellant systems. The characterization of CARS spectroscopy obtained from these studies was used to obtain initial CARS measurements from the reaction zone of nitramine composite propellant flames. These studies are only possible using a coherent, highly spatially, and temporally resolved spectroscopy such as CARS. These qualities of CARS which have been applied to the deflagration of propellants containing the explosive ingredients nitrocellulose and/or RDX can be used to study the decomposition and explosive reactions of other energetic materials in both the gas and solid phases.

CONTENTS

TABLES

FIGURES

INTRODUCTION

Obtaining useful experimental information on the dynamics of deflagration and detonation of energetic materials has been difficult with conventional optical techniques. The advent of nonlinear optical techniques such as coherent anti-stokes Raman scattering (CARS) provides an opportunity to extend the information obtainable on these energetic systems. Propellant flames are often transient, particle-laden, incandescent, and, under some conditions, turbulent. However, single-shot nitrogen CARS spectra from propellant flames have been obtained (refs 1 and 2). This use of CARS in obtaining temperature and concentration from propellant flames led to further investigations in the model propellant flames from CH_4/N_2O (refs 3, 4, and 5).

CARS spectroscopy (ref 6, 7, and 8) has several features which are especially suitable for probing propellant flames. These include recent modifications which have enhanced the usefulness of CARS for investigating flames. CARS arises from the nonlinear response of homogeneous media. The nonlinear response, when beams ω_1 and ω_2 are incident, generates an oscillating polarization. The lowest order nonlinearity is the third order susceptibility, $\chi^{(3)}(-\omega_3, \omega_1, \omega_1 - \omega_2)$,

which generates a frequency component of the polarization at $\omega_3 = 2\omega_1 - \omega_2$. Vibrational resonant enhancement of this three-wave mixing process occurs if $\omega_1 - \omega_2$ is made equal to a Raman-active vibration, in which case the enhancement of the signal ω_3 is a CARS process. Since CARS is a coherent process, ω_3 is maximized if the wave-vectors, k_i, are phasematched so that $k_1 = k_2 + k_3$ where k_i equals $\omega_i n_i/c$, c the speed of light, and n_i the refractive index at frequency ω_i. In gases, which are nearly dispersionless, colinear beams are phasematched. With colinear geometry, the spatial resolution is poor since CARS is generated by an iterative growth process.

If ω_1 is split and phasematching is achieved, ω_3 is maximized and, since CARS generation occurs only where all three beams intersect, the spatial resolution is improved. The split ω_1 phasematching is termed BOXCARS. BOXCARS, in which the wave vectors are not phasematched in one plane, is termed folded (or nonplanar) BOXCARS and has the advantage that ω_3 is easily separated spatially from the generating beams. BOXCARS can easily be constituted so that the effective sampling volume in the flame is less than 1-mm in the direction of the laser beams and 200 microns in cross section in the transverse direction.

ω_2, when narrowband, is scanned to obtain the spectrum at ω_3. However, to obtain spectra in transient and/or turbulent media, it is appropriate to use a broadband ω_2 [~150 cm^{-1} full width at half height (FWHH)] to obtain the full rovibrational spectrum at ω_3 within the time duration of the laser pulse (~10 ns). Averaging of the single-shot broadband spectra can be used to improve the signal-to-noise in some experiments. The coherence of CARS, together with the spatial resolution of BOXCARS and the time resolution of broadband spectra is

necessary to probe propellant flames. Broadband BOXCARS was the configuration used to obtain the first propellant CARS spectra (ref 1). Some aspects of propellant flames and those features of CARS needed for probing propellant flames will be discussed in further detail. The CARS spectra obtained from both the reaction zone and post-flame regions of the CH_4/N_2O model propellant flame will be discussed in terms of their applicability to future propellant flame studies. Initial CARS measurements on nitramine propellants using the spatial resolution of CARS to probe the propellant reaction zone will also be discussed.

PROPELLANT FLAMES

The propellant flames that are of primary interest in this work are those generated by burning solid propellants formulated primarily from nitrocellulose/ nitroglycerin (which are termed double-base propellants) and from nitramines such as RDX (1, 3, 5 trinitro hexahydro 1, 3, 5, triazine). Both double-base and nitramine propellant modelings were recently reviewed by Miller (ref 9).
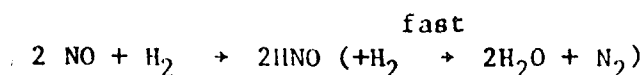
In double-base propellants, it is thought that the solid decomposes to NO_2, aldehydes, and other similar small molecules (foam zone). These react further to give principally NO, CO, H_2, N_2, CO_2 and small organic fragments (fizz or dark zone). Finally, the NO and CO react further to give the luminous flame (flame zone) (ref 10). Heller and Gordon (ref 10) used fine thermocouples imbedded both in the propellant and close to the propellant surface to measure the temperature distribution. A temperature of 600 to 800 K was measured at the propellant surface. The dark zone gas temperature rose as a result of the fizz zone reactions to about 1500 K at low pressure (40 psi). This rise in dark zone temperature to 1500 K occurred within about 1-mm of the propellant surface at 40 psi. In an inert atmosphere, the luminous flame zone appears about 15-mm above the propellant surface as the pressure is raised to 10 to 15 atm.

Similar results in terms of dimensions of the gas flame zones were obtained by Zenin in 1966 (ref 11) and earlier by Crawford et al in 1950 (ref 12) for propellant burning in an inert atmosphere where it was shown that the length of the dark zone is inversely proportional to the cube root of the pressure. Crawford also observed propellant burning in air at atmosphere pressure (ref 12). When ignited with a flame, propellant burned in air with a luminous flame. Ignition with a hot wire resulted in flameless burning (fizz burning) with the same burning rate. Since the burning rate was the same in using both methods of ignition, the rate-controlling processes in the solid or close to the surface were assumed to be the same. The luminous flame, although it does increase the overall heat released from the propellant, apparently does not contribute substantially to the heat release at the propellant surface which controls the rate of burning at atmospheric pressure.

Heller and Gordon (ref 10) have also measured the composition of the gas in the dark zone at 150 psi and 200 psi using small sampling probes. The composition measured was H_2 (10%), CO (40%), N_2 (5%), NO (30%), and CO_2 (15%).

The double base, fizz-zone reaction has been attributed by Scotter (ref 13) to reactions between nitrogen dioxide, glyoxal, formaldehyde, formic acid, hydro-

2

gen cyanide, and nitrous acid. The most important process leading to the luminous flame are thought to be (ref 13)

$$H_2O + H \rightarrow H_2 + OH$$

$$CO + OH \rightarrow CO_2 + H$$

$$2\ NO + H_2 \xrightarrow{\text{fast}} 2HNO\ (+H_2 \rightarrow 2H_2O + N_2)$$

The pressure dependence of the burning rate of the double-base propellant is thus attributed to the termolecular nature of the nitric oxide-hydrogen reaction (ref 13). Previously Crawford et al (ref 12) had observed that the burning rate of double-base propellant flames closely fit an expression of the form

$$r = a + b\ P_n$$

where r is the burning rate; P the pressure; and a, b, and n are constants characteristic of the powder composition. The pressure-independent and pressure-dependent terms were associated with reactions occurring in the solid and the gas phase, respectively. Double-base propellant flames have recently been modeled in the Beckstead-Derr-Price (BDP) framework by Beckstead (ref 14).

NITRAMINE PROPELLANTS

Nitramine propellants contain a substantial percentage of nitramines (75%) along with a varying percentage of energetic binders (nitrocellulose) and/or nonenergetic binders (organic ester). Current models of nitramine propellant combustion are essentially models of HMX (cyclotetranithylene tetranitramine) and RDX deflagration. The burning rate expression for nitramine propellants (ref 15)

$$r = ap^{1/2}\ (1 + p/b)^{1/2}$$

is such that at low pressure

$$p \ll b,\ r \sim p^{1/2}$$

whereas at high pressure

$$p \gg b,\ r \sim p^1$$

Much of the modeling of nitramine propellant has been to explain this complex burning rate behavior.

Ben-Reuuen and Summerfield (ref 16) have recently reviewed nitramine propellant modeling and have derived improvements to the comprehensive Ben-Reuuen and Caveny (ref 15) model of nitramine deflagration (refs 15 and 17). The Ben-Reuuen and Caveny model consists of the following chemical mechanism:

First, partial decomposition of RDX in the liquid phase

$$RDX(L) \rightarrow 3CH_2O + 9/4\ N_2O + 3/4\ NO + 3/8\ N_2$$
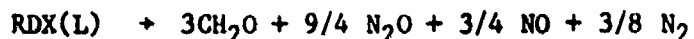
Second, gas phase decomposition of RDX in the near field (close to the propellant surface)

$$RDX(G) \rightarrow NO_2 + N_2O + 3CH_2O + 3/2\ N_2$$
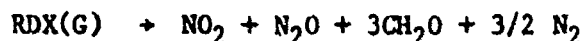
Third, oxidation of formaldehyde by NO_2

$$CH_2O + NO_2 \rightarrow H_2O + CO + N_2$$

in the far field (relatively far from the propellant surface).

Detailed thermocouple temperature profiles in the nitramine solid are not available, as they are in nitrocellulose propellants, to estimate the length of the various reaction zones. However, the calculations of Ben-Reuuen and Caveny (ref 15) indicate that the near field at 10 atm is within tens of microns of the propellant surface. If the length of the near field of nitramine propellants scales similarly to the dark zone of nitrocellulose propellant (i.e., as the cube of the pressure) at atmospheric pressure, the near field should be of the order to millimeters.

Ben-Reuuen and Summerfield (ref 16) have added to the Ben-Reuuen and Caveny model a nonequilibrium evaporation low at the melt/gas interface, an improved melt phase model including decomposition-gas bubble, and model for far-field processes, with several simultaneous secondary reactions.

Schroeder (ref 18) has recently reviewed nitramine decomposition chemistry. At low temperature (500 to 600 K), the gas phase reaction mechanism by which RDX initially decomposes to CH_2O and N_2O is postulated as

$$(CH_2NNO_2)_3 \rightarrow 3CH_2O + 3N_2O$$

This is thought to occur through HONO elimination and/or cyclic decomposition via the intermediate N-nitroformaimine, CH_2NNO_2. Crossover to a high temperature reaction mechanism in the gas phase is thought to occur above about 600 K. This mechanism is thought to occur via breakage of an initial HN bond followed by fragmentation to CH_2NNO_2 which decomposes to HCN and NO_2, leading to the overall initial reaction

$$(CH_2NNO_2)_3 \rightarrow 3HCN + 6NO_2 + 3H_2$$

The liquid phase reaction is also thought to occur by a mechanism similar to the high temperature gas phase reaction mechanism.

Price et al (ref 19) have recently modified the BDP model for RDX to incorporate both the high (endothermic) and low (exothermic) temperature mechanisms in the solid and exothermic and endothermic second order reactions in the gas phase.

CARS APPARATUS

A CARS spectrometer appropriate for studying both the model and actual propellant flames is shown in figure 1 and is described in detail in reference 5. Nonplanar BOXCARS was utilized to achieve phasematching. The output of a Quanta-Ray DCR-1A Nd/YAG laser at 1.06 μm (700 mJ) is doubled to generate the pump beam at 5320A (250 mJ) with a bandwidth of near 1 cm^{-1}. The pump beam is split with beam splitter BS1 to generate ω_{1s}. ω_{1s} is used to pump a dye laser to generate the Stokes beam, ω_2, with a bandwidth of about 130 cm^{-1} and an energy of about 30 mJ. To achieve BOXCARS geometry, ω_{1p} is again split with beam splitter, BS2, to generate ω_1 and ω_1'. In the optical configuration used to generate nonplanar BOXCARS, the ω_1, ω_1', and ω_2 beams are parallel and situated on a circle at the focusing lens. To achieve phasematching, an optical flat was inserted into ω_2 before focusing. After collimation, ω_3 is spatially isolated and focused into a monochromator. The signal was detected by a PAR SIT detector and processed by a PAR OM2 system.

CARS THEORY

The observed CARS spectrum is proportional to the square of the modulus of the third-order susceptibility, $\chi^{(3)}$, which is the sum of a resonant term χ_r (related to nuclear displacements) and a nonresonant term χ_{nr} (related to electronic displacement)

$$\chi^{(3)} = \chi_r + \chi_{nr} \tag{1}$$

The resonant term is calculated as a sum of Lorentzian line shapes of each Q(J) rovibrational transition,

$$\chi_r = \sum_j \frac{k_j \Gamma_j}{2 \Delta_j - i\Gamma_j} \tag{2}$$

given that

$$k_j = (2N/h)|\alpha_j|(\Delta p_j)\Gamma_j^{-1} \tag{3}$$

where N is the number density, α_j is the polarization matrix element for the transition, Δp_j is the normalized population difference between the molecular energy levels involved in the transition, Γ is the isolated pressure-broadband linewidth, and $\Delta_j = \omega_1 - \omega_2 - \omega_j$. The calculated $|\chi^{(3)}|^2$ is first convoluted over the laser shapes and then over a triangular-instrumental slit function.

χ_r is the sum of real and imaginary components χ' and χ'', respectively, such that

$$|\chi^{(3)}|^2 = \chi'^2 + 2\chi' \chi_{nr} + \chi''^2 + \chi_{nr}^2 \qquad (4)$$

χ' and χ'' display dispersive and resonant behavior, respectively, with respect to the detuning frequency Δ_j.

As the contribution of the squared resonant terms in equation 4 is lowered, the cross term $\chi' \chi_{nr}$, which is dispersive, modulates the shapes of the spectrum. The squared resonant contribution is decreased with lowered concentration of the resonant species and lowered population difference, Δp_j. The extent of modulation of a Q-branch will increase for a given concentration as the temperature is raised since the ratio of resonant to nonresonant signal at a given frequency is decreased due to population of hot bands. The lowest intensity, hot bands will exhibit the largest cross-term modulation. Thus, the shape of the total CARS spectrum is a complicated function of temperature and concentration. Approximate temperature can be extracted from the CARS spectrum by considering only those features which are relatively much more intense than the nonresonant susceptiblity. At constant temperature, concentration can be obtained from the ratio of total CARS intensity, I, to the nonresonant intensity, I_{nr}, at a particular frequency (ref 5).

To calculate CARS spectra according to the above procedure, the spectral and linewidth parameters of the resonant species and the nonresonant susceptiblity of all the species present at significant concentration (above about 1%) must be known. In the post-flame region of hydrocarbon flames, these parameters are known to some degree for the predominant species CO, CO_2, N_2, and H_2O (ref 7). In propellant flames, many of the species thought to be present in various zones of propellant (i.e., NO, NO_2, HCN, N_2O) have not as yet had CARS spectra and models thereof reported (except as discussed below for N_2O). Additionally, H_2 is present at temperatures (3000 K) and concentrations (30%) such that pure rotational S-branch transitions are seen in many regions of the propellant CARS spectra.

RESULTS AND DISCUSSION

Post-Flame Zone

The N_2 CARS spectra (fig. 2) was obtained from the post-flame region of a double-base propellant flame (refs 1 and 2). This spectrum was taken to demonstrate the feasibility of obtaining CARS spectra from a propellant flame. The spectrum, however, shows several features not common to CARS spectra obtained from hydrocarbon/air flames. The temperature, estimated as 2500 K ± 150 K based on the height of the first hot band, is higher than that usually encountered in hydrocarbon/air flames. A prominant second hot band is encountered at 2282 cm^{-1}. The shape of the spectrum can be consistently interpreted if it is assumed that there is substantial cross-term modulation (CARS Theory section). This is consistent with the concentration of N_2 (10%) and temperature (2600 K) estimated from thermochemical calculations (ref 2). Since propellant flames, in general, have a lower concentration of N_2 (usually less than 30%) than hydrocarbon/air flames (where N_2 concentration is about 70%), N_2 CARS spectra obtained from pro-

pellant are, in general, more strongly affected by cross-term modulation than N_2 CARS spectra from hydrocarbon/air flames.

For this reason, N_2 CARS spectra were obtained from a series of CH_4/N_2O flames (ref 5). The experimental and thermochemically calculated (NASA-LEWIS CODE) temperatures and concentrations of N_2 are given in table 1 for lean and stoichiometric flames. An example of the fit of the experimental data to the calculated CARS spectra is given in figure 3.

These measurements have been extended to rich CH_4/N_2O flames which closely resemble propellant flames for N_2 and CO CARS (Harris, et al, ref 20, and Aron et al, ref 21). The results for both N_2 and CO are in close agreement with thermochemical calculations for unshielded flames provided the flames are not too rich ($\phi < 1.5$). These rich flames ($\phi > 1.5$) were found to give temperature and concentration in agreement with thermochemical calculations when properly shielded. In addition, in these flames hydrogen-pure rotational transitions were observed in the positions noted in table 2. CO and N_2 CARS, the nonresonant background and the 2139 cm^{-1} S_0 (11,9) pure rotational H_2 transition atop the CO Q (1,0) band are shown in figure 4. The transitions were initially assigned with the spectroscopic constants of Fink et al (ref 22). A better correlation of the theory and experiment given in table 2 was found using spectroscopic constants obtained from potential functions calculated from ab initio calculation utilizing a generalized James-Coolidge wavefunction (ref 23). In general, propellant flames will show a series of sharp rotational lines which are spaced by a varying interval on the order of a hundred wave numbers throughout the CARS spectrum due to both the relatively high concentration and temperature of H_2. These lines are presently beng modeled to allow prediction of H_2 temperature and concentration from CARS S-branch rotational spectra (ref 23). Additionally, the H_2 Q-branch can be used to obtain similar information. The hydrogen-pure rotations offer the advantage of allowing simultaneous spectra with a number of other species (i.e., CO, NO, CO_2), assuring that the relative concentrations of the species pertain to the same spatial and temporal location in the flame.

Thus, present results from both actual and model propellant flames for N_2 and CO suggest that CARS spectra can be used to assess the ability of thermodynamic calculations to predict propellant post-flame zone flame conditions. Comparison in the post-flame region to thermochemical calculation should be particularly interesting as the pressure at which the propellant is burned varies.

Reaction Zone

To assess the utility of CARS for making measurements in the reaction zone, simultaneous N_2 and N_2O CARS spectra shown in figure 5 were obtained from the reaction zone of 0.3 equivalence ratio CH_4/N_2O flames (refs 4 and 5). Spectra were obtained from room temperature to near the adiabatic flame temperature. Simultaneous spectra are especially valuable from the reaction zone since it is characterized by sharp spatial and temperature gradients. Simultaneous spectra assure the coincidence of the spatial and temporal location of the resonant species, thus improving the kinetic validity of the data. However, the data reduction of simultaneous spectra is complicated by cross-term interaction of the

resonant species. The effect of cross-term interactions of the resonant species is dependent on the frequency separation of the resonant species. The spectra shown in figure 4 directly demonstrates that CARS has the capability of detecting chemical changes occurring in a distance of less than 100 microns. Thus, the spatial resolution of CARS is sufficient to directly provide information to help to understand the chemical changes occurring in the reaction zone. The temperatures and concentrations obtained from the spectra shown in figure 5 were consistent with attributing the low temperature (T<1700 K) flame decomposition of N_2O to the reaction

$$H + N_2O \rightarrow N_2 + OH$$

where $k = 6 \times 10^{13} \exp(-13100/RT) \ cm^3 \ mole^{-1}s^{-1}$

This reaction has been invoked to explain mass spectrometric data from the H_2/N_2O flame (ref 24) although the recently reported rate for the reaction of CH and N_2O, $(7.8 \pm 1.4) \times 10^{-11} \ cm^3 \ s^{-1}$ at 300 K (ref 25) may lead to more quantitative interpretation of the data.

The spatial resolution obtained in the reaction zone of CH_4/N_2O flames indicates that CARS has the potential for probing, in favorable cases, the initial gas phase reactions that occur within 1 mm of the surface of burning nitrocellulose or nitramine propellant. The secondary reactions, which occur within 15 mm of the surface in nitrocellulose propellant flames at low pressure and the post-flame region, are well within the spatial resolution of CARS. CARS spectra obtained in the initial and secondary reaction zones will be difficult to interpret quantitatively because of the necessity of (1) knowing all the species present to determine the nonresonant susceptibility (2) determining spectral parameters for species previously uncharacterized. However, even qualitatively in-situ information will be useful for suggesting the reaction mechanisms responsible for propellant burning. Propellant reaction zone studies must be performed at the lowest pressures necessary for propellant combustion because of the inverse cubic dependence of the reaction zone length with pressure.

The post-flame region should present fewer difficulties since thermodynamic calculations are available to give estimates of gas composition for making initial estimates of the nonresonant susceptibility. Measurements at higher pressure should permit sufficiently high signal strength to allow cancellation of the nonresonant background (ref 7) giving temperature independent of composition.

Preliminary results have been obtained (ref 26) from the initial and/or secondary gas phase reaction zone and flame zone of a composite nitramine propellant (isobaric flame temperature, 2064 K; flame composition: 5% CO_2, 37% CO, 9% H_2O, 28% H_2, and 22% N_2) formulated for low vulnerability to ignition. The composite nitramine is 76% RDX, 20% organic esters, and 4% nitrocellulose. The products of organic ester decomposition would be expected to dilute the neat RDX decomposition products, such that the dark zone would be lengthened and the burning rate consequently slowed. The CARS spectra obtained from the surface of the propellant (that is, the spectra taken as close to the surface as possible) qualitatively show lower-than-equilibrium concentrations of final products (N_2, CO, and a number of intermediate species including HCN) and temperature not inconsistent with estimated surface temperature of 600 to 700 K (Propellant Flame section). Higher above the surface (6 mm), the intermediates decrease and the tem-

perature and concentrations of final products increase (as shown in the CARS spectra given in figure 6). At the surface, strong signals are seen from H_2, CO, and HCN, whereas at 6 mm the HCN signal is diminished with respect to both the CO and H_2 signals. Still higher (20 mm), the concentration and temperature of N_2 is near the calculated thermodynamic values. These results are consistent with a mechanism of RDX decomposition in which HCN is an early or first product. Thus, the results in both the reaction zone of CH_4/N_2O flames and nitramine propellant flames indicate that CARS has the capability of providing direct, in-situ information on species concentration and temperature in the reaction zone of reactive media.

CONCLUSIONS

CARS spectra obtained from propellant flames have several features not commonly encountered in spectra obtained from hydrocarbon/air flames upon which most of the previous CARS flame studies have centered. Hydrocarbon/air flames have a high concentration of N_2 (near 70%), such that temperature can be obtained from the nitrogen CARS spectra without undue concern for cross-term concentration modulation. In contrast, propellant flames often do not have any final product at a concentration much above 30%. As a consequence, temperature and concentration must be extracted simultaneously from the dominant final products of propellant combustion (N_2, CO, and H_2). Studies in CH_4,N_2O flames have shown that this can be done with good precision for both N_2 and CO. Preliminary studies in the post-flame region of nitrocellulose and nitramine propellant flames also indicate that temperature and concentration can be obtained with good precision. These post-flame propellant results should be compared to thermochemical calculations as a function of pressure. Additionally, propellant flames show a series of sharp rotational lines spaced by a varying interval on the order of a hundred wave numbers. These lines are due to pure rotations resulting from the relatively high concentration and temperature of H_2. These lines are useful because they allow simultaneous observation of hydrogen concentration relative to that of other species; i.e., NO, CO, CO_2, and offer straightforward temperature determination.

CARS spectra provide a means, as demonstrated in model and actual propellant flames, of providing precise temperature and concentration profiles through the various zones of propellant combustion. Even the qualitative information provided by CARS on the chemical species present in the initial gas phase decomposition (close to the propellant surface) provides otherwise unobtainable insight into the reactions determining propellant burning. This initial decomposition zone, which is less than 1 mm even at ambient pressure, and the secondary gas phase decomposition zone, which is of the order of 15-mm at ambient pressure, are most profitably studied at the lowest pressures consistent with propellant burning. These studies are only possible with a coherent, highly spatially, and temporally resolved spectroscopy such as CARS. These qualities which have been applied to the deflagration of propellants containing the explosive ingredient nitrocellulose and/or RDX can be extended to other reactive and explosive reactions of other energetic material in both the gas and solid phases.

9

REFERENCES

1. L. E. Harris and M. E. McIwain, "Coherent Anti-Stokes Raman Spectroscopy in Propellant Flames," *Fast Reactions in Energetic Systems*, D. Capellos and R. F. Walker, ed., Reidel, Boston, MA, 1981, pp 473-434.

2. L. E. Harris and M. E. McIlwain, *Combustion and Flame*, vol 48, 1982, pp 97-100.

3. L. E. Harris, *Chemical Physics Letters*, vol 93, 1982, pp 335-340.

4. L. E. Harris, "CARS Spectra from Lean and Stoichiometric CH_4/N_2O Flames," Technical Report ARLCD-TR-82026, ARRADCOM, Dover, NJ, March 1983.

5. L. E. Harris, "CARS Spectra from Lean and Stoichiometric CH_4/N_2O Flames," *Combustion and Flame*, 1983, in press.

6. S. A. J. Druet and J. P. E. Taran, "CARS Spectroscopy," *Progress in Quantum Electronics*, vol 7, 1981, pp 1-72.

7. A. C. Ecbreth and P. Schreiber, "Coherent Anti-Stokes Raman Spectroscopy (CARS): Application to Combustion and Gas-Phase Diagnostics," *Chemical Application of Nonlinear Raman Spectroscopy*, A. B. Arvey, ed., Academic Press, New York, NY, 1981, pp 27-87.

8. J. W. Nibler and G. V. Knighten, "Coherent Anti-Stokes Raman Spectroscopy," *Raman Spectroscopy of Gases and Liquids*, A. Weber, ed., Springer-Verlag, Berlin, 1979, pp 253-299.

9. M. S. Miller, *Combustion and Flame*, vol 6, 1982, pp 51-73.

10. C. A. Heller and A. S. Gordon, *Journal of Physical Chemistry*, vol 59, 1955, p 773.

11. A. A. Zenin, *Fizika Goreniyai Vzryva*, vol 2, 1966, pp 67-76.

12. B. L. Crawford, C. Huggett, and J. J. McBrady, *Journal of Physical Chemistry*, vol 54, 1950, p 854.

13. J. G. Scotter, "Chemical Kinetics of the Cordite Explosion Zone," Proceedings of Tenth International Symposium on Combustion, Combustion Institute, Pittsburgh, PA, 1965, pp 1405-1411.

14. M. W. Beckstead, *AIAA Journal*, vol 18, 1980, pp 980-985.

15. M. Ben-Reuuen and L. H. Caveny, "Nitramine Flame Chemistry and Deflagration Interpreted in Terms of a Flame Model," *AIAA Journal*, vol 19, 1981, pp 1276-1285.

16. M. Ben-Reuuen and M. Summerfield, "Combustion of Nitramine Propellants," Technical Report ARBRL-CR-00507, ARRADCOM, Dover, NJ, March 1983.

17. M. Ben-Reuuen, L. H. Caveny, R. Bichnevetsky, and M. Summerfield, "Flame Zone and Subsurface Reaction Model for Deflagrating RDX," Proceedings of Sixteenth International Symposium on Combustion, Combustion Institute, Pittsburgh, PA, 1976, pp 1223-1233.

18. M. A. Schroeder, "Critical Analysis of Nitramine Decomposition Data Product Distribution from HMX and RDX Decomposition," Proceedings of the Eighteenth JANNAF Combustion Meeting, CPIA Publication No. 347, 1981, pp 395-413.

19. C. F. Price, T. L. Boggs, T. P. Parr, and D. M. Parr, "A Modified BDP Model Applied to the Self-Deflagration of HMX," Proceedings of the Nineteenth JANNAF Combustion Meeting, CPIA Publication No. 366, 1982, pp 299-310.

20. L. E. Harris, K. Aron, and J. Fendell "N_2 and CO Vibrational CARS and H_2 Rotational CARS Spectroscopy of CH_4/N_2O Flames," Proceedings of the Nineteenth JANNAF Combustion Meeting, CPIA Publication No. 366, 1982, p 123.

21. K. Aron, L. E. Harris, and J. Fendell, "N_2 and CO Vibrational CARS and H_2 Rotational CARS Spectroscopy of CH_4/N_2O Flames," Appl. Optics, 1983, in press.

22. U. Fink, T. Wiggins, and D. Rank, Journal of Molecular Spectroscopy, vol 18, 1965, p 384.

23. J. Fendell, L. E. Harris, and K. Aron, "Theoretical Calculation of H_2 CARS S-Branches for Propellant Flames," Proceedings of the Twentieth JANNAF Combustion Meeting, 1983.

24. V. P. Balakhnine, J. Vandooron, and P. J. VanTiggelen, Combustion and Flame, vol 28, 1977, p 165.

25. S. S. Wagel, T. Carrinton, S. V. Fiolseth, and C. M. Sadowski, Chemical Physics Letters, vol 69, 1982, p 61.

26. K. Aron and L. E. Harris, "CARS Studies of RDX Combustion and Decomposition," Chemical Physics Letters, 1983, in press.

Table 1. Measured and calculated temperature (K) and N_2 concentration (%) in CH_4/N_2O flames

Height[a] (mm)	Gas flow (cm/s)	Fuel oxidizer (equivalence ratio)	Temperature (K)		N_2 Concentration (%)	
			Experimental	Calculated	Experimental	Calculated
5	16.8	0.3	2550	2541	60	62
2	16.8	0.4	2688	2654	58	60
2	33.4	0.5	2782	2738	54	58
2	51.7	1.0	2982 ± 52 (2%)[b]	2920	45 ± 3 (6%)[b]	51

[a] Height above the surface of the barrier.

[b] Percentage error of the measurement.

Table 2. H_2 rotational CARS transitions observed in CH_4/N_2O and nitramine propellant flames

Transition (J', J'')	Experimental (cm^{-1})		Calculated (cm^{-1})	
	v = 0	v = 1	v = 0	v = 1
7, 5	1446	----	1447	1374
9, 7	1809	1714	1815	1721
11, 9	2131	(2010)	2130	2019

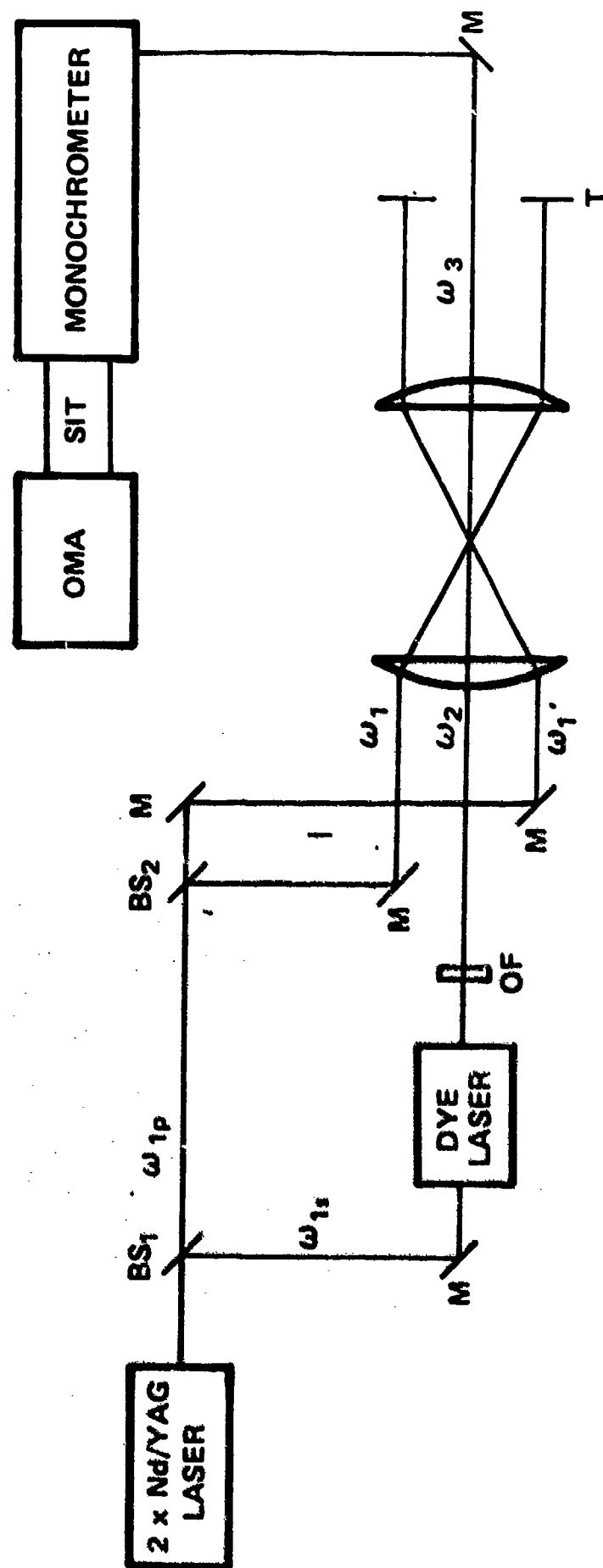Figure 1. Nonplanar BOXCARS spectrometer where BS is a 50% beam splitter, M is a mirror, OF is an optical flat rotatable about its horizontal axis, and T is a beam terminator

15
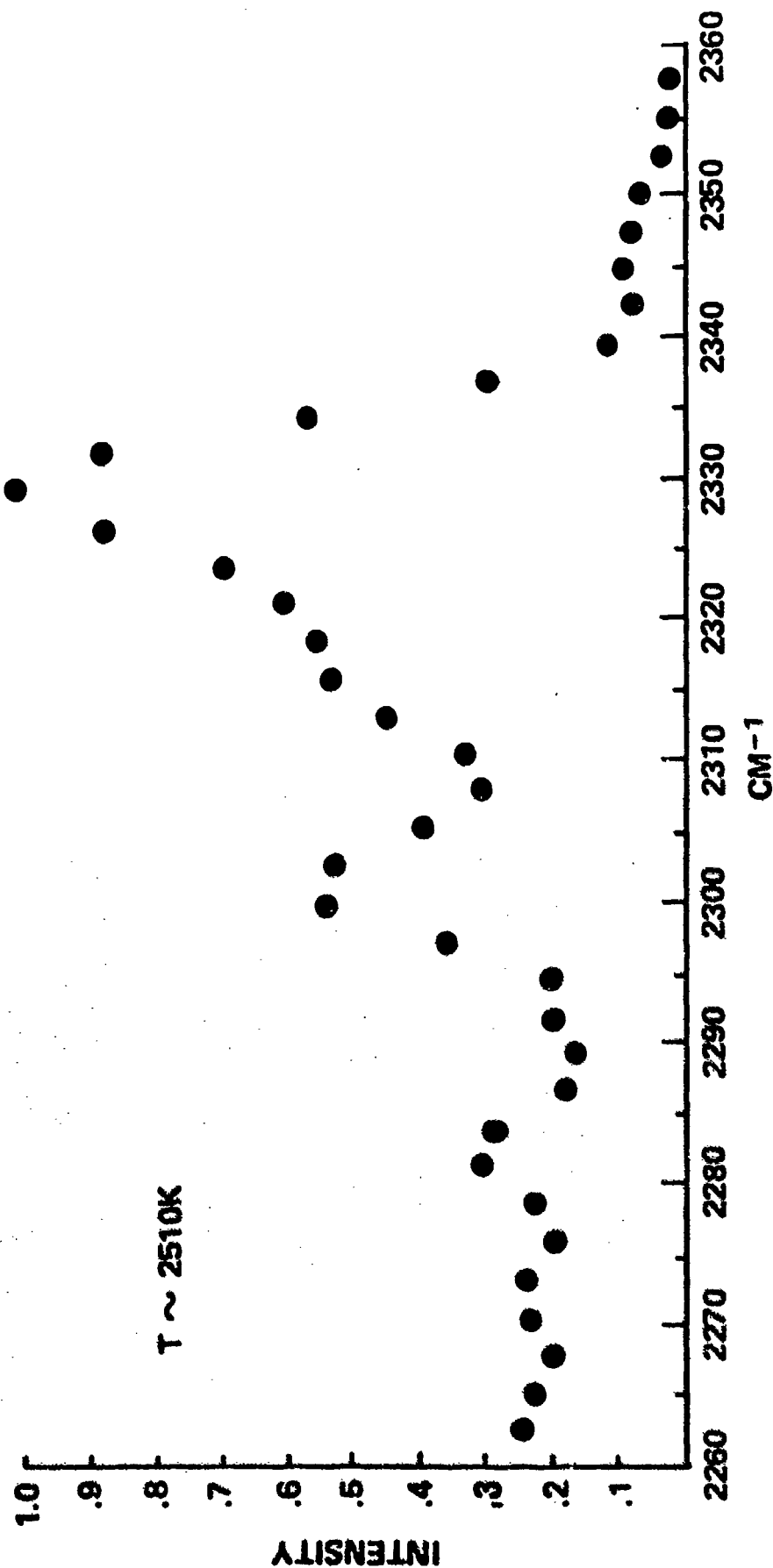
Figure 2. CARS nitrogen spectrum from a double-base propellant flame burning unconfined in air. The spectrum was taken using a single laser pulse 10-mm above the centerline of the propellant surface. I_{max} = 212 counts, T = 2500 ± 150 K.
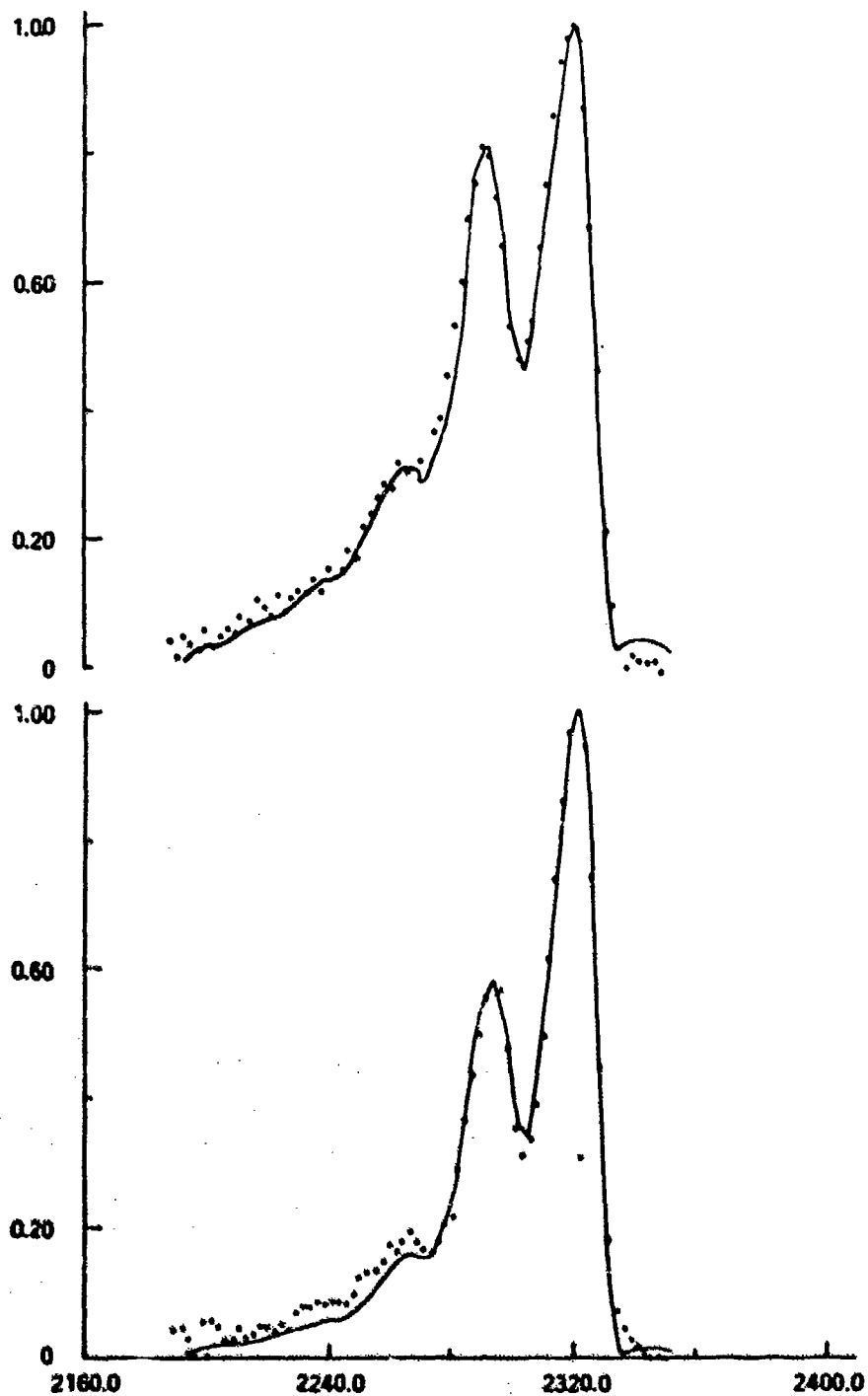
Figure 3. CARS spectrum observed 2-mm above the burner head (·) compared with a
theoretical spectrum (solid line) calculated for 2688 K and 58% N_2 for
a ϕ = 0.4 flame (bottom spectrum); 2982 K and 45% for a ϕ = 1.0 flame
(top spectrum).
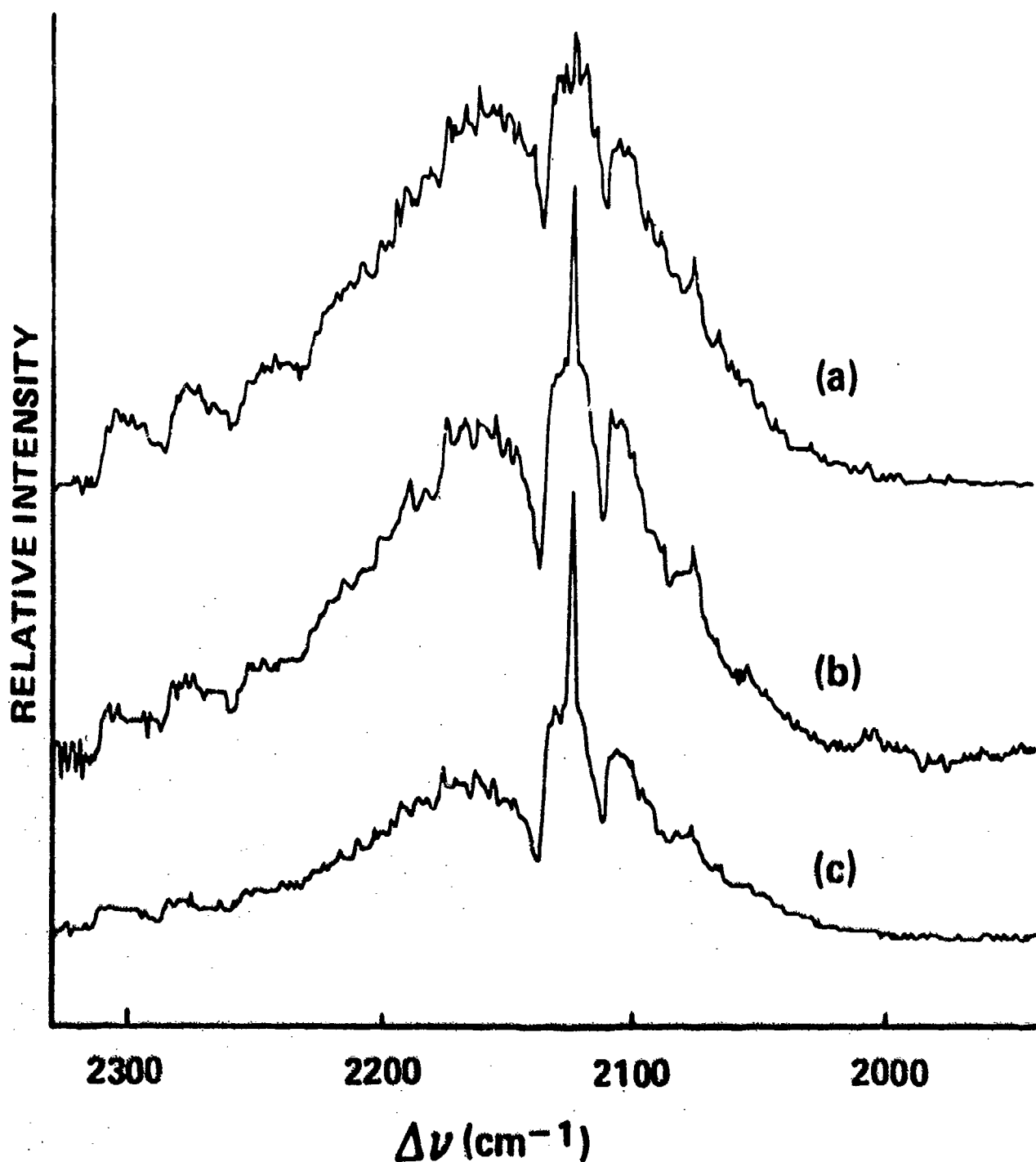
Figure 4. CARS spectrum of CO region for (a) ϕ = 1.2 flames; (b) ϕ = 1.8 flame; and (c) ϕ = 2.5 flame. The CO and N_2 resonant and nonresonant susceptibility. The narrow peak at 2131 cm^{-1} atop the CO Q (1,0) band is the hydrogen, pure rotational S_o (11,9) transition.
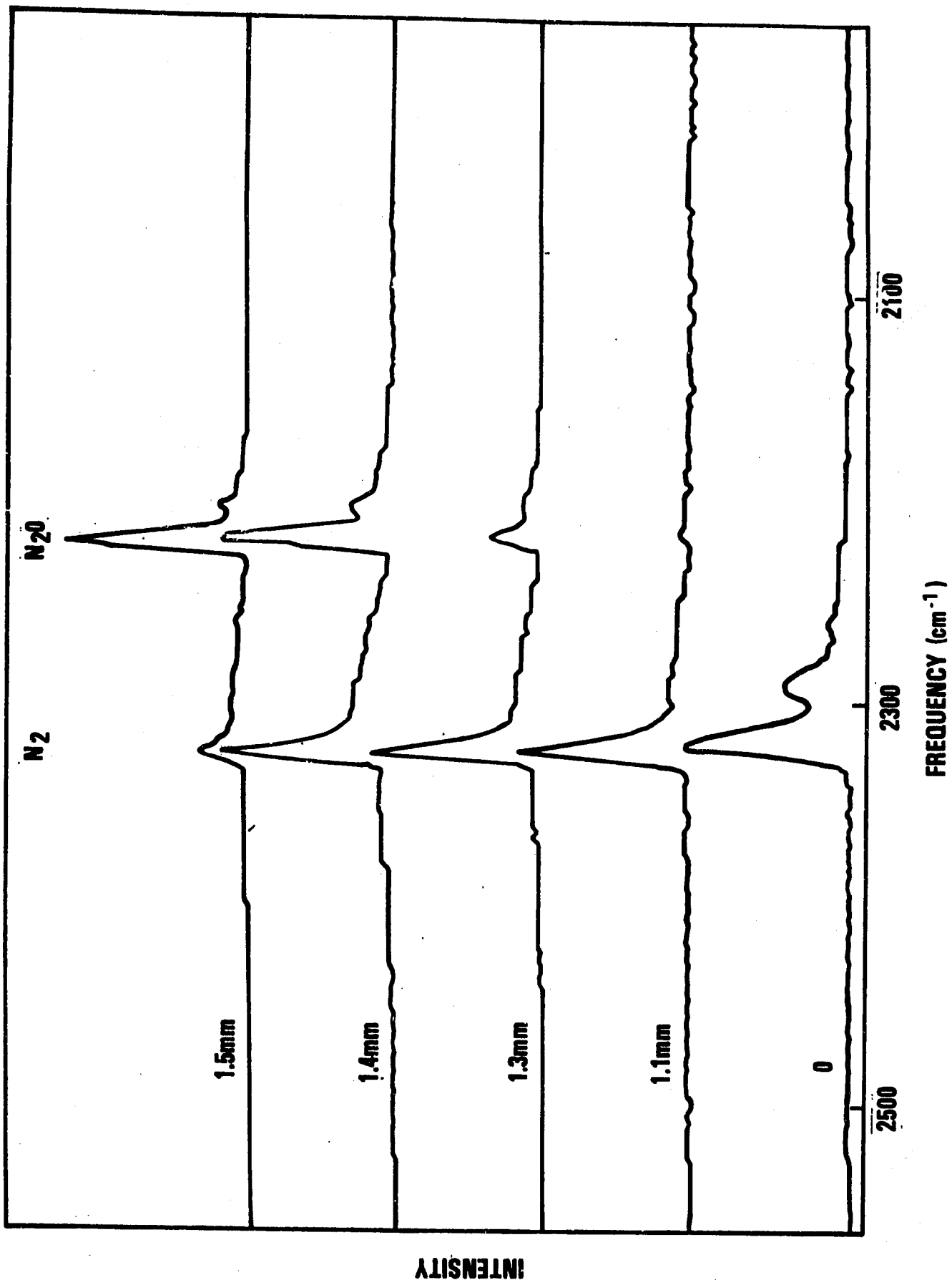
Figure 5. CARS spectra observed 1-mm above the burner head in a 0.27 CH_4/N_2O flame. The distance indicated is from the centerline of the burner.

19

RAMAN FREQUENCY (CM—1)

RELATIVE INTENSITY
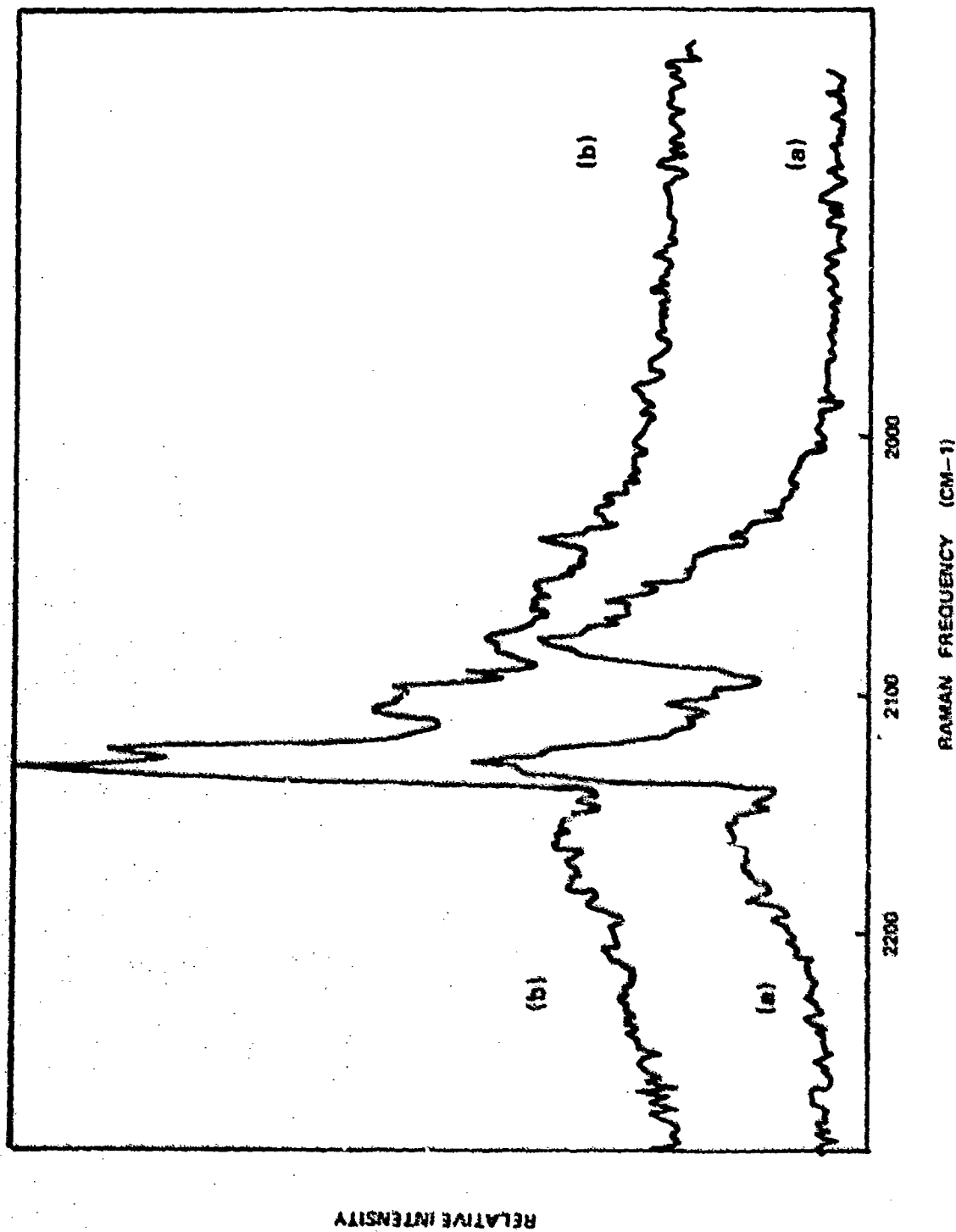
Figure 6. (a) The single-shot CARS spectrum at the nitramine surface.
           (b) The averaged CARS spectrum at a height of 6-mm above the nitramine surface in the
                region $\Delta\nu \approx 2100$ cm^{-1}. At the surface, strong signals are seen from H_2 S_o (11,9)
                at 2131 cm^{-1}, the CO Q (1,0) at 2137, and HCN Q (1,0) at 2087 cm^{-1}, whereas the
                HCN signal is diminished at 6-mm with respect to both the CO and H_2 signals.

20

Commander
Armament Research and Development Center
U.S. Army Armament, Munitions and
   Chemical Command
ATTN: DRSMC-TSS(D) (5)
      DRSMC-TDC(D), L. A. Gyorog
      DRSMC-GCL(D)
      DRSMC-LC(D), J. Frasier
               J. P. Picard
      DRSMC-LCA(D), T. Davidson
      DRSMC-LCA-C(D), J. Lannon
               D. Downs
               L. Harris (10)
               T. Vladimiroff
               A. Beardell
               Y. Carignon
               J. Fendell
               K. Aron
               E. Petro
      DRSMC-LCE(D), R. Walker
               P. Marinkas
               C. Capellos
               F. Owens
               S. Bulusu
               F. Gilbert
Dover, NJ 07801

Administrator
Defense Technical Information Center
ATTN: Accessions Division (12)
Cameron Station
Alexandria, VA 22314

Director
U.S. Army Materiel Systems
  Analysis Activity
ATTN: DRXSY-MP
Aberdeen Proving Ground, MD 21005

Commander
Chemical Research and Development Center
U.S. Army Armament, Munitions and
   Chemical Command
ATTN: DRSMC-CLJ-L(A)
      DRSMC-CLB-PA(A)
APG, Edgewood Area, MD 21010

Director
Ballistics Research Laboratory
Armament Research and Development Center
U.S. Army Armament, Munitions and
    Chemical Command
ATTN: DRSMC-TSB-S(A)
       DRSMC-BLP(A), L. Watermier
                     A. Barrows
                     G. Adams
                     R. Fifer
                     M. Miller
                     T. Coffee
                     J. Heimeryl
                     C. Nelson
                     J. Vanderhoff
                     J. Anderson
Aberdeen Proving Ground, MD 21005

Chief
Benet Weapons Laboratory, LCWSL
Armament Research and Development Center
U.S. Army Armament, Munitions and
    Chemical Command
ATTN: DRSMC-LCB-TL
Watervliet, NY 12189

Commander
U.S. Army Armament, Munitions and
    Chemical Command
ATTN: DRSMC-LEP-L(R)
Rock Island, IL 61299

Director
U.S. Army TRADOC Systems
    Analysis Activity
ATTN: ATAA-SL
White Sands Missile Range, NM 88002

Director
Defense Advanced Research Projects
    Agency
ATTN: LTC C. Buck
1400 Wilson Boulevard
Arlington, VA 22209

Commander
U.S. Army Materiel Development
    and Readiness Command
ATTN: DRCMD-ST
5001 Eisenhower Avenue
Alexandria, VA 22333

Commander
U.S. Army Watervliet Arsenal
ATTN: SARWV-RD, R. Thierry
Watervliet, NY 12189

Director
U.S. Army Air Mobility Research
    and Development Laboratory
Ames Research Center
Moffett Field, CA 94035

Commander
U.S. Army Communications Research
    and Development Command
ATTN: DRDCO-PPA-SA
Fort Monmouth, NJ 07703

Commander
U.S. Army Electronics Research
    and Development Command
Technical Support Activity
ATTN: DELSD-L
Fort Monmouth, NJ 07703

Commander
U.S. Army Missile Command
ATTN: DRSMI-R
      DRSMI-YDL
Redstone Arsenal, AL 35809

Commander
U.S. Army Natick Research
    and Development Command
ATTN: DRXRE, D. Sieling
Natick, MA 01762

Commander
U.S. Army Tank Automotive Research
    and Development Command
ATTN: DRDTA-UL
Warren, MI 48090

Commander
U.S. Army White Sands Missile Range
ATTN: STEWS-VT
White Sands Missile Range, NM 88002

Commander
U.S. Army Materials and
    Mechanics Research Center
ATTN: DRXMR-ATL
Watertown, MA 02172

Commander
U.S. Army Research Office
ATTN: Technical Library
        D. Squire
        F. Schmiedeshaff
        R. Ghirardelli
        M. Ciftan
P.O. Box 12211
Research Triangle Park, NC 27706

Office of Naval Research
ATTN: Code 473
       G. Neece
800 N. Quincy Street
Arlington, VA 22217

Commander
Naval Sea Systems Command
ATTN: J. W. Murrin, SEA-62R2
National Center
Bldg 2, Room 6E08
Washington, DC 20362

Commander
Naval Surface Weapons Center
ATTN: Library Branch, DX-21
Dahlgren, VA 22448

Commander
Naval Surface Weapons Center
ATTN: Code 240, S. J. Jacobs, J. Sharma
       Code 730
Silver Spring, MD 20910

Commander
Naval Underwater Systems Center
Energy Conversion Department
ATTN: Code 5B331, R. S. Lazar
Newport, RI 02840

Commander
Naval Weapons Center
ATTN: R. Derr
       C. Thelen
China Lake, CA 93555

Commander
Naval Research Laboratory
ATTN: Code 6180
Washington, DC 20375

Superintendent
Naval Postgraduate School
ATTN: Technical Library
       D. Netzer
       A. Fuhs
Monterey, CA 93940

Commander
Naval Ordnance Station
ATTN: Dr. Charles Dale
       Technical Library
Indian Head, MD 20640

AFOSR
ATTN: J. F. Masi
       B. T. Wolfson
       D. Ball
       L. Caveny
Bolling AFB, DC 20332

AFRPL (DYSC)
ATTN: D. George
       J. N. Levine
Edwards AFB, CA 93523

National Bureau of Standards
ATTN: J. Hastie
       T. Kashiwagi
       H. Semerjian
       M. Jacox
       K. Smyth
       J. Stevenson
Washington, DC 20234

Lockheed Palo Alto Research Laboratories
ATTN: Technical Information Center
3521 Hanover Street
Palo Alto, CA 94304

Aerojet Solid Propulsion Co.
ATTN: P. Micheli
Sacramento, CA 95813

ARO Incorporated
ATTN: N. Dougherty
Arnold AFS, TN 37389

Atlantic Research Corporation
ATTN: M. K. King
5390 Cherokee Avenue
Alexandria, VA 22314

25

AVCO Corporation
AVCO Everett Research Laboratory
   Division
ATTN: D. Stickler
2385 Revere Beach Parkway
Everett, MA 02149

Calspan Corporation
ATTN: E. B. Fisher
       A. P. Trippe
P.O. Box 400
Buffalo, NY 14221

Foster Miller Associates, Inc.
ATTN: A. J. Erickson
135 Second Avenue
Waltham, MA 02154

General Electric Company
Armament Department
ATTN: M. J. Bulman
Lakeside Avenue
Burlington, VT 05402

General Electric Company
Flight Propulsion Division
ATTN: Technical Library
Cincinnati, OH 45215

Hercules Incorporated
Alleghany Ballistic Lab
ATTN: R. Miller
       Technical Library
Cumberland, MD 21501

Hercules Incorporated
Bacchus Works
ATTN: B. Isom
Magna, UT 84044

IITRI
ATTN: M. J. Klein
10 West 35th Street
Chicago, IL 60615

Olin Corporation
Badger Army Ammunition Plant
ATTN: J. Ramnarace
Baraboo, WI 53913

Olin Corporation
New Haven Plant
ATTN: R. L. Cook
       D. W. Riefler
275 Winchester Avenue
New Haven, CT 06504

Paul Gough Associates, Inc.
ATTN: P. S. Gough
P.O. Box 1614
Portsmouth, NH 03801

Physics International Company
2700 Merced Street
Leandro, CA 94577

Pulsepower Systems, Inc.
ATTN: L. C. Elmore
815 American Street
San Carlos, CA 94070

Rockwell International Corp.
Rocketdyne Division
ATTN: C. Obert
       J. E. Flanagan
       A. Axeworthy
6633 Canoga Avenue
Canoga Park, CA 91304

Rockwell International Corp.
Rocketdyne Division
ATTN: W. Haymes
       Technical Library
McGregor, TX 76657

Science Applications, Inc.
ATTN: R. B. Edelman
Combustion Dynamics and
   Propulsion Division
23146 Cumorah Crest
Woodland Hills, CA 91364

Shock Hydrodynamics, Inc.
ATTN: W. H. Anderson
4710-16 Vineland Avenue
N. Hollywood, CA 91602

Thiokol Corporation
Elkton Division
ATTN: E. Sutton
Elkton, MD 21921

Thiokol Corporation
Huntsville Division
ATTN:　D. Flanigan
　　　　R. Glick
　　　　Technical Library
Huntsville, AL　35807

Thiokol Corporation
Wasatch Division
ATTN:　J. Peterson
　　　　Technical Library
P.O. Box 524
Brigham City, UT　84302

TRW Systems Group
ATTN:　H. Korman
One Space Park
Redondo Beach, CA　90278

United Technologies
Chemical Systems Division
ATTN:　R. Brown
　　　　Technical Library
P.O. Box 358
Sunnyvale, CA　94086

Battelle Memorial Institute
ATTN:　Technical Library
　　　　R. Bartlett
505 King Avenue
Columbus, OH　43201

Brigham Young University
Department of Chemical Engineering
ATTN:　N. W. Beckstead
Provo, UT　84601

California Institute of Technology
204 Karman Lab
Mail Stop 301-46
ATTN:　F. E. C. Culick
1201 E. California Street
Pasadena, CA　91125

Case Western Reserve University
Division of Aerospace Sciences
ATTN:　J. Tien
Cleveland, OH　44135

Georgia Institute of Technology
School of Aerospace Engineering
ATTN: B. T. Zinn
       E. Price
       W. C. Strahle
Atlanta, GA 30332

Institute of Gas Technology
ATTN: D. Gidaspow
3424 S. State Street
Chicago, IL 60616

Johns Hopkins University/APL
Chemical Propulsion Information Agency
ATTN: T. Christian
Johns Hopkins Road
Laurel, MD 20810

Massachusetts Institute of Technology
Department of Mechanical Engineering
ATTN: T. Toong
Cambridge, MA 02139

Pennsylvania State University
Applied Research Laboratory
ATTN: G. M. Faeth
P.O. Box 30
State College, PA 16801

Pennsylvania State University
Department of Mechanical Engineering
ATTN: K. Kuo
University Park, PA 16801

Pennsylvania State University
Department of Material Sciences
ATTN: H. Palmer
University Park, PA 16801

Princeton Combustion Research
   Laboratories
ATTN: M. Summerfield
       N. Messina
1041 U.S. Highway One North
Princeton, NJ 08540

Princeton University
Forrestal Campus
ATTN: I. Glassman
       F. Dryer
       Technical Library
P.O. Box 710
Princeton, NJ 08540

Purdue University
School of Mechanical Engineering
ATTN: J. Osborn
       S. N. B. Murthy
       N. M. Laurendeau
TSPC Chaffee Hall
W. Lafayette, IN 47906

Rutgers State University
Department of Mechanical and
   Aerospace Engineering
ATTN: S. Temkin
University Heights Campus
New Brunswick, NJ 08903

SRI International
ATTN: Technical Library
       D. Crosley
       J. Barker
       D. Golden
333 Ravenswood Avenue
Menlo Park, CA 94025

Stevens Institute of Technology
Davidson Library
ATTN: R. McAlevy, III
Hoboken, NJ 07030

United Technology
ATTN: Alan Ecbreth
       Robert Hall
Research Center
East Hartford, CT 06108

Commander
Naval Research Laboratory
Chemistry Division
ATTN: A. Harvey
Washington, DC 20375

General Motors Research Laboratory
ATTN: J. H. Bechtel
Warren, Michigan 48090

System Research Laboratory
ATTN: L. Goss
2600 Indian Ripple Rd
Dayton, Ohio 45440

Exxon Research and Engineering
ATTN: A. Dean
       M. Chou
P.O. Box 45
Linden, NJ   07036

Ford Motor Company
Research Staff
ATTN: K. Marko
       L. Rimai
Dearborn, Michigan   48120

Sandia Laboratories
Applied Physics Division I
ATTN: L. Rahn
       D. Stephenson
Livermore, CA   94550

Rensselaer Polytechnic Institute
Dept. of Chem. Engineering
ATTN: A. Fontijn
Troy, NY   12181

University of California,
San Diego
Ames Department
ATTN: F. Williams
P.O. Box 109
La Jolla, CA   92037

University of California
Dept. of Mechanical Eng.
ATTN: J. W. Daily
Berkeley, CA   94720

University of Dayton
University of Dayton Research Inst.
Dayton, OH   45406

University of Florida
Dept. of Chemistry
ATTN: J. Winefordner
Gainesville, Florida   32601

University of Illinois
Dept. of Mechanical Eng.
ATTN: H. Krier
144 MEB, 1206 W. Green St.
Urbana, IL   61801

University of Minnesota
Dept. of Mechanical Eng.
ATTN: E. Fletcher
Minneapolis, MN 55455

University of California,
Santa Barbara
Quantum Institute
ATTN: K. Schofield
M. Steinberg
Santa Barbara, CA 93106

University of Southern California
Department of Chemistry
ATTN: S. Benson
Los Angeles, CA 90007

Stanford University
Department of Mech. Eng.
ATTN: R. Hanson
Stanford, CA 93106

University of Texas
Department of Chemistry
ATTN: W. Gardiner
H. Schaefer
Austin, TX 78712

University of Utah
Dept. of Chemical Engineering
ATTN: A. Baer
G. Flandro
Salt Lake City, UT 84112